Self-Assembly of Antimicrobial Peptides on Gold Nanodots: Against Multidrug-Resistant Bacteria and Wound-Healing Application

Wei-Yu Chen, Hsiang-Yu Chang, Jenn-Kan Lu, Yi-Cheng Huang, Scott G. Harroun, Yu-Ting Tseng, Yu-Jia Li, Chih-Ching Huang, and Huan-Tsung Chang**

Photoluminescent gold nanodots (Au NDs) are prepared via etching and codeposition of hybridized ligands, an antimicrobial peptide (surfactin; SFT), and 1-dodecanethiol (DT), on gold nanoparticles (≈3.2 nm). As-prepared ultrasmall SFT/DT–Au NDs (size ≈2.5 nm) are a highly efficient antimicrobial agent. The photoluminescence properties and stability as well as the antimicrobial activity of SFT/DT–Au NDs are highly dependent on the density of SFT on Au NDs. Relative to SFT, SFT/DT–Au NDs exhibit greater antimicrobial activity, not only to nonmultidrug-resistant bacteria but also to the multidrug-resistant bacteria. The minimal inhibitory concentration values of SFT/DT–Au NDs are much lower (>80-fold) than that of SFT. The antimicrobial activity of SFT/DT–Au NDs is mainly due to the synergistic effect of SFT and DT–Au NDs on the disruption of the bacterial membrane. In vitro cytotoxicity and hemolysis analyses have revealed superior biocompatibility of SFT/DT–Au NDs than that of SFT. Moreover, in vivo methicillin-resistant *S. aureus*–infected wound healing studies in rats show faster healing, better epithelialization, and are more efficient in the production of collagen fibers when SFT/DT–Au NDs are used as a dressing material. This study suggests that the SFT/DT–Au NDs are a promising antimicrobial candidate for preclinical applications in treating wounds and skin infections.

1. Introduction

Bacterial infections cause health problems and even death for millions of people worldwide.[1] Common antibiotics such as ampicillin, erythromycin, gentamycin, sodium sulfacetamide, benzoyl peroxide, and azelaic acid are used against the growth or to kill bacteria.[2] Unfortunately, bacterial resistance to conventional medical antibiotics and a range of adverse side effects associated with inappropriate antibiotic treatment and overuse of antibiotics are serious problems.[3] Antimicrobial peptides, known as natural antibiotics, can combat drug-resistant bacteria, mainly because their distinctive amino sequences can insert into and subsequently disintegrate bacterial cell surfaces.[4,5] However, they are usually cytotoxic and hemolytic to human cells and erythrocytes, respectively.

Antimicrobial nanomaterials, such as silver, copper oxide, zinc oxide, and titanium dioxide nanoparticles (NPs) have emerged as potential alternatives for the treatment of drug-resistant bacterial infections.[6,7] The high antimicrobial activity of metallic and metal oxide NPs, with their small sizes and high surface area, is mainly attributed to their large contact area with bacteria that leads to the destruction of the permeability and respiration functions of bacteria membranes.[8] In addition, the penetrated NPs and/or ions released from their surfaces may further interact with proteins, DNA and RNA molecules, which inhibits cellular functions.[8] Moreover, reactive oxygen species (ROS) generated due to NPs may also induce damage to cells.[8] The complex antimicrobial mechanisms of metallic and metal oxide NPs greatly reduce the

W.-Y. Chen, H.-Y. Chang, S. G. Harroun, Y.-T. Tseng, Prof. H.-T. Chang
Department of Chemistry
National Taiwan University
Taipei 10617, Taiwan
E-mail: changht@ntu.edu.tw
Prof. J.-K. Lu
Department of Aquaculture
National Taiwan Ocean University
Keelung 20224, Taiwan
Prof. Y.-C. Huang
Department of Food Science
National Taiwan Ocean University
Keelung 20224, Taiwan
Y.-J. Li, Prof. C.-C. Huang
Department of Bioscience and Biotechnology
National Taiwan Ocean University
Keelung 20224, Taiwan
E-mail: huanging@ntou.edu.tw
Prof. C.-C. Huang
Center of Excellence for the Oceans
National Taiwan Ocean University
Keelung 20224, Taiwan
Prof. C.-C. Huang
School of Pharmacy, College of Pharmacy
Kaohsiung Medical University
Kaohsiung 80708, Taiwan

DOI: 10.1002/adfm.201503248

probability of bacteria developing drug resistance to them.[9] Although metallic and metal oxide NPs exhibit high potential for treatment of drug-resistant bacteria, they are toxic to most human cells, which limits their use.[10] To minimize toxic effects, NPs conjugated with antibiotics, carbon-based nanomaterials, and multifunctional upconverting nanoparticles have been prepared.[11] In addition, they provide synergistic effects, which enhance their antimicrobial activities.[11]

Molecular (noncovalent) self-assembly of functional ligands on NP surfaces can provide dense recognition units for multivalent interactions with biological molecules, or for cooperative binding to different receptors on cell surfaces.[12] The high local concentration of recognized ligands on NP surfaces can also enhance their binding affinity and specificity toward targets.[13] Small-sized gold nanomaterials are stable and nontoxic, and have become one of the most attractive cores for preparation of biofunctional nanomaterials.[14] Self-assembled oligonucleotides, peptides, and oligosaccharides on gold nanomaterials possess plasmonic absorption, photoluminescence, catalytic activity, and have been shown to be useful for biosensing, cell labeling, and therapy of tumor cells.[14] They are, however, rarely applied for antimicrobial applications,[15] mainly because of the low antimicrobial nature of gold nanomaterials.

In this work, we have prepared antimicrobial gold nanodots (Au NDs; ≈2.5 nm) coimmobilized with surfactin (SFT) and 1-dodecanethiol (DT). We have previously reported that the deposition of alkanethiols onto the surfaces of gold nanoparticles (Au NPs; ≈3.2 nm) results in the formation of photoluminescent Au NDs.[16] SFT, a cyclic lipopeptide with a sequence of Glu-Leu-D-Leu-Val-Asp-D-Leu-Leu linked by a lactone bond to a C11–15 β-hydroxy fatty acid (**Scheme 1**A), provides antimicrobial, antiviral, antifungal, antimycoplasma, and hemolytic activities.[17,18] It penetrates cellular membranes mainly through its cation-carrier, pore-forming, and detergent effects.[19] The hybrid SFT/DT-capped Au NDs (SFT/DT–Au NDs) were prepared through self-assembly of antimicrobial peptides (SFT) on DT-anchored Au NDs by the nonspecific hydrophobic interactions between the alkyl chains of the SFT and DT molecules (Scheme 1A). The as-prepared SFT/DT–Au NDs were characterized by UV–vis absorption and photoluminescence spectroscopy, transmission electron microscopy (TEM), zeta potential (ζ), and electrospray ionization quadrupole time-of-flight mass spectrometer (ESI-Q-TOF MS) measurements. Relative to SFTs and DT–Au NDs, SFT/DT–Au NDs possessed superior antimicrobial activity toward non-multi-drug resistant (non-MDR) bacteria, such as *Escherichia coli* (*E. coli*), *Proteus vulgaris* (*P. vulgaris*), *Salmonella enterica serovar Enteritidis* (*S. enteritidis*), and *Staphylococcus aureus* (*S. aureus*), as well as multidrug resistant (MDR) bacteria like *methicillin-resistant S. aureus* (MRSA). MRSA is a type of *Staphylococcus* bacterium, and it is resistant to many antibiotics commonly used to treat ordinary *Staphylococcus* infections, including methicillin, nafcillin, and oxacillin.[20] The water dispersibility, photoluminescence, as well as antimicrobial activity of Au NDs are highly dependent on the ligand ratio of SFT/DT on their surfaces. In vivo results demonstrated that the antibacterial wound-healing effect of SFT/DT–Au NDs is superior to that of SFT on an MRSA-infected wound in rats. Furthermore, in vitro hemolysis and cytotoxicity analyses of SFT/DT–Au NDs revealed their insignificant hemolysis in red blood cells (RBCs) and low toxicity in selected cell lines [immortalized human breast epithelial cell line (MCF-10A), mouse embryonic fibroblast

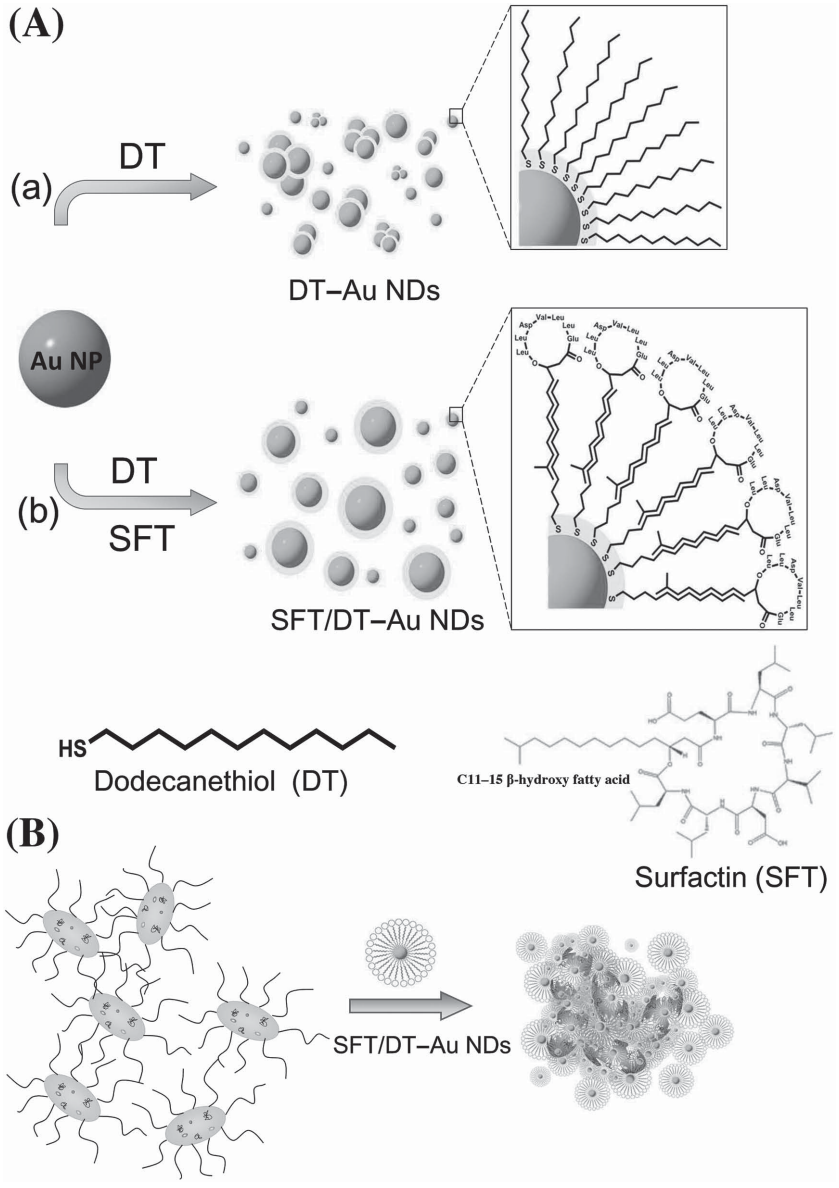

Scheme 1. A) Synthesis of photoluminescent SFT/DT–Au NDs and B) their antimicrobial activity through the SFT-mediated disruption of bacterial cells.

cell line (NIH-3T3), and human microvascular endothelial cell line (HMEC-1)].

2. Results and Discussion

2.1. Characterization of SFT/DT–Au NDs

Tetra(hydroxymethyl)phosphonium chloride (THPC) was used as a reducing agent and a capping agent to prepare Au NPs (≈3.2 nm) from $AuCl_4^-$ in alkaline solution.[21] The surface of the Au NPs were functionalized with DT ligands or DT/SFT hybrid ligands, which induced their dissolution (etching). As a result, Au–thiolate complexes were formed on the surfaces of Au cores, with an average particle size of 2–3 nm. For simplicity, these as-prepared SFT/DT–Au NDs are denoted as $SFT_{0.05}$/DT–Au NDs, $SFT_{0.1}$/DT–Au NDs, $SFT_{0.25}$/DT–Au NDs, $SFT_{0.5}$/DT–Au NDs, and $SFT_{1.0}$/DT–Au NDs that were prepared using the SFT/DT ligands at concentrations of 0.05/1.0, 0.1/1.0, 0.25/1.0, 0.5/1.0, and $1.0/1.0 \times 10^{-3}$ M, respectively. **Figure 1** displays the UV–vis absorption and photoluminescence spectra of the as-prepared DT–Au NDs and SFT/DT–Au NDs. The absorption band of Au NDs in the near-UV region arises from the hybrid electronic states involved with ligand–metal (S—Au) charge transfer and/or mixture with ligand-to-metal–metal charge transfer of $(—S—Au(I)—S—Au(I)—S—)_n$ staples constructed from various Au—Au and Au—S bonds on the Au ND surfaces.[22] In aqueous solution, DT is immiscible; however, SFT/DT complexes formed through the hydrophobic interactions of DT with SFT are miscible. As a result, it is relatively easier for the SFT/DT complexes than for DT to access the surfaces of Au NPs. When compared to DT–Au NDs, SFT/DT–Au NDs have smaller particle sizes (Figure S1, Supporting Information; **Table 1**) and exhibit higher absorbance in the UV region (Figure 1A). Compared to DT–Au NDs (≈3 nm), $SFT_{0.5}$/DT–Au NDs having larger hydrodynamic size (≈10.5 nm), implying SFT molecules are assembled on DT–Au NDs (Figure S2, Supporting Information). The ESI-Q-TOF MS spectra of purified $SFT_{0.5}$/DT–Au NDs (Figure S3, Supporting Information) show peaks at m/z 1008.77, 1022.79, and 1036.81, which are assigned for SFTs with alkyl chains of C_{10}, C_{11}, and C_{12}, respectively, further supported the existence of SFT molecules on the Au ND surfaces.

The photoluminescence of DT–Au NDs is a combination that arises from the Au ND core and the Au(I)–SR shell.[23,24] The energy level of the highest occupied molecular orbital (HOMO) in the hybrid states (p-orbitals of S and 6sp orbitals of the surface Au atoms/ions) of the as-prepared Au NDs are lower than that of the d-band of surface Au atoms and ions.[25] Therefore, the visible-emitted photoluminescence of the Au NDs (≈510 nm) could possibly arise mainly from sp- to d-band transitions of the Au cores. However, the photoluminescence properties of Au NDs are highly dependent on the density and charge of their capping shells.[25] The dense capping–ligand shell of SFT/DT on the surface of Au NDs can minimize their collision with quenchers (e.g., oxygen molecules, halide ions) and the internal nonradiative relaxation pathways (which restrain intramolecular vibrations and rotations).[26] As a result, the photoluminescence intensity of the SFT/DT–Au NDs is much stronger than that of the DT–Au NDs (Figure 1B); the photoluminescence intensity increases upon increasing the concentration of SFT used in the preparation of Au NDs and reaches a plateau at the SFT concentration of 1.0×10^{-3} M. The photoluminescence quantum yields (Φ_f) of DT–Au NDs and $SFT_{1.0}$/DT–Au NDs are 1.19% and 3.01% (Table 1), respectively. A slight blue shift of the emission of SFT/DT–Au NDs (Figure 1B) is probably due to their smaller particle size, which results in a larger band gap of the sp- to d-band transitions.[25] The shorter photoluminescence lifetimes (τ_1/τ_2; Figure S4, Supporting Information) and higher ratio of Au(I) in the Au NDs (Table 1) that had been prepared in the presence of higher concentration of SFT are consistent with their stronger absorption, smaller sizes, and densely packed ligand shell. The electron-donating feature of SFT may enhance the ligand-to-metal charge transfer (S→Au) on the surfaces and therefore contributes to their higher absorption coefficient, photoluminescence intensity, and shorter lifetime.[27]

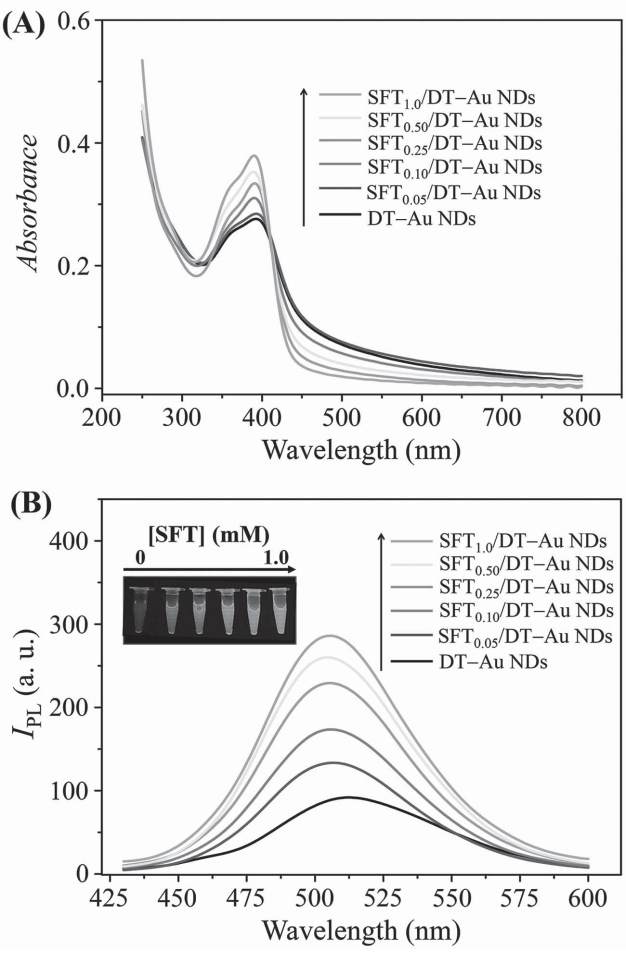

Figure 1. A) UV–vis absorption and B) emission spectra of DT–Au NDs and SFT/DT–Au NDs ([Au NDs] = 100×10^{-9} M) in 5.0×10^{-3} M sodium phosphate solution (pH 7.4). The SFT/DT–Au NDs were obtained from the reactions of THPC–Au NPs (≈3.2 nm; 0.5×10^{-6} M) with DT (1.0×10^{-3} M), and DT (1.0×10^{-3} M)/SFT ($0.05–1.0 \times 10^{-3}$ M) in 20×10^{-3} M sodium tetraborate (pH 9.2) at ambient temperature for 48 h, respectively. Inset in (B): photograph of the DT–Au NDs and five SFT/DT–Au NDs solutions upon excitation under a handheld UV lamp (365 nm). Photoluminescence intensities (I_{PL}) in (B) are plotted in arbitrary units (a.u.). Excitation wavelengths in (B) for DT–Au NDs and SFT/DT–Au NDs were set at 390 nm.

Table 1. Sizes, oxidation states [Au(I)/Au(0)], and optical properties of DT–Au NDs and SFT/DT–Au NDs prepared from Au NP solutions at DT (1.0×10^{-3} M) and various concentrations of SFT (0–1.0×10^{-3} M).

Au NDs	Size [nm]	λ_{max}^{em} [a)] [nm]	QY [%]	Au(I)/Au(0)	Absorption coefficient [b)] [ε, M^{-1} cm^{-1}]	Lifetime [τ_1/τ_2, ns]
DT–Au NDs	3.03 ± 0.19	512	1.19	64.1/35.9	2.67×10^5	105.3 (51.2%)/14.8 (48.8%)
$SFT_{0.05}$/DT–Au NDs	2.87 ± 0.46	507	2.10	66.3/33.7	2.84×10^5	90.2 (57.8%)/14.4 (42.2%)
$SFT_{0.1}$/DT–Au NDs	2.52 ± 0.26	506	2.37	69.2/30.8	3.10×10^5	89.1 (59.2%)/13.2 (40.8%)
$SFT_{0.25}$/DT–Au NDs	2.43 ± 0.29	505	2.68	73.4/26.6	3.34×10^5	88.1 (57.1%)/12.5 (42.9%)
$SFT_{0.5}$/DT–Au NDs	2.20 ± 0.29	505	2.94	77.6/22.4	3.53×10^5	86.4 (59.3%)/10.6 (40.7%)
$SFT_{1.0}$/DT–Au NDs	2.02 ± 0.21	506	3.01	80.2/19.8	3.79×10^5	84.0 (63.5%)/9.4 (36.5%)

[a)]Emission-band maxima upon excitation at a wavelength of 390 nm; [b)]Absorption coefficient at the wavelength of the absorption-band maxima.

2.2. Antimicrobial Properties SFT/DT–Au NDs

Because photoluminescent SFT/DT–Au NDs had ultrasmall particle sizes and highly dense antimicrobial peptide (SFT) ligands on their surface, they were used to inhibit bacteria growth. The minimal inhibitory concentration (MIC) values of the SFT and SFT/DT–Au NDs were determined by a standard dilution method in various tested bacterial strains (**Figure 2**), including one non-MDR Gram-positive (*S. aureus*), three non-MDR Gram-negative (*S. enteritidis*, *E. coli*, and *P. vulgaris*), and one MDR Gram-positive (MRSA) bacteria. The inhibitory activities of SFT/DT–Au NDs are not only effective against the four non-MDR bacterial strains but also the MDR bacterial strain. We found that the inhibitory activities of SFT/DT–Au NDs increased upon increasing the concentration of SFT. The results suggested that the antimicrobial properties of SFT/DT–Au NDs exhibited synergistic effects from SFT and the DT–Au NDs. Among the prepared SFT/DT–Au NDs, $SFT_{0.5}$/DT–Au NDs exhibited the best inhibitory activity against the tested bacterial strains. The MIC value (in terms of the concentration of SFT) of $SFT_{0.5}$/DT–Au NDs (3×10^{-6} M) for MDR strain (MRSA) is >80-fold lower than that of SFT (≈250×10^{-6} M). Relative to $SFT_{0.5}$/DT–Au NDs (MIC < 0.003×10^{-6} M Au NDs), the much weaker inhibitory activity of DT–Au NDs (MIC > 1.0×10^{-6} M Au NDs) is ascribed to its low solubility. The $SFT_{1.0}$/DT–Au NDs showed slightly lower antimicrobial activity than $SFT_{0.5}$/DT–Au NDs (Figure 2), mainly because a large amount of free SFT molecules competed with SFT/DT–Au NDs to interact with the bacteria.

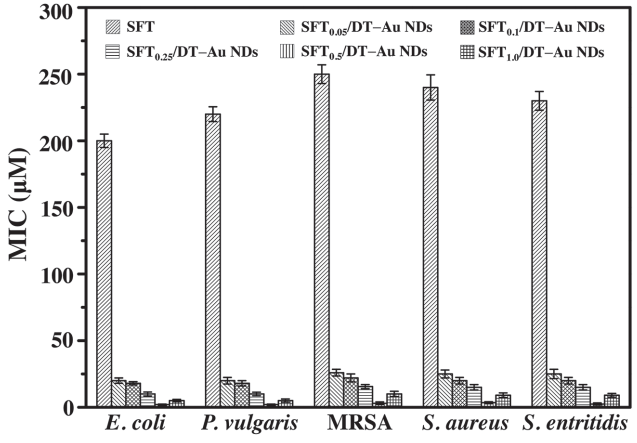

Figure 2. Comparison of minimum inhibitory concentrations (MICs; in terms of the concentration of SFT) of surfactin, $SFT_{0.05}$/DT–Au NDs, $SFT_{0.1}$/DT–Au NDs, $SFT_{0.25}$/DT–Au NDs, $SFT_{0.5}$/DT–Au NDs, and $SFT_{1.0}$/DT–Au NDs against five bacteria (*E. coli*, *P. vulgaris*, MRSA, *S. aureus*, and *S. enteritidis*). Error bars represent the standard deviation of three repeated measurements.

Inhibition zone measurements were further conducted to assess the antimicrobial activity of SFT, DT–Au NDs, and $SFT_{0.5}$/DT–Au NDs. Figure S5 (Supporting Information) reveals that the $SFT_{0.5}$/DT–Au NDs-loaded cellulose thin film (diameter = 0.8 cm) exhibited a much larger inhibition zone (2.60 ± 0.30 and 1.80 ± 0.20 cm) for *E. coli* and *S. aureus* than those of SFT (0.15 ± 0.08 and 0.08 ± 0.03 cm) and DT–Au NDs (0.10 ± 0.05 and 0.05 ± 0.01 cm), respectively. In contrast to DT–Au NDs, the bacteria provided bright photoluminescence after they interacted with $SFT_{0.5}$/DT–Au NDs (Figure S6, Supporting Information). The photoluminescence feature of Au NDs allows using SFT/DT–Au NDs to label bacteria for cellular imaging applications without any modification. Nanoparticles conjugated with fluorophores are widely used to investigate cellular uptake of nanoparticles, internalization, and subcellular localization of nanoparticles.[28] The optical resolution of tracing of Au NDs into/in cells should be better than that of most fluorescent nanoparticles having the sizes >10 nm, mainly because of their small particle size (<3 nm). The inductively coupled plasma mass spectrometry (ICP-MS) measurement (with regard to elemental Au) reveals the amount of $SFT_{0.5}$/DT–Au NDs (≈250 Au NDs per *bacterium*) conjugated to *E. coli* was ≈20-fold higher than that of DT–Au NDs (≈12 Au NDs per *E. coli bacterium*). Our result suggests the SFT ligands on Au NDs play a crucial role in the interaction of SFT/DT–Au NDs with the bacteria.

2.3. Disruption of Bacterial Membranes

The antimicrobial properties of $SFT_{0.5}$/DT–Au NDs via generation of intracellular ROS is excluded, with a support no fluorescent product formed from 2′,7′-dichlorodihydrofluorescein diacetate (DCFDA) dye. DCFDA can be deacetylated to the non-fluorescent 2′,7′-dichlorodihydrofluorescein (DCF) by cellular

esterases and then oxidized by ROS into fluorescent DCF with maximum excitation and emission spectra of 495 and 529 nm, respectively.[29] transmission electron microscopy (TEM) and scanning electron microscopy (SEM) measurements were conducted to explore the mechanism of the antimicrobial activities of the $SFT_{0.5}$/DT–Au NDs against bacteria. It is generally accepted that the antimicrobial properties of amphiphilic SFT molecules is due to destabilization of the bacterial membranes and interruption of their integrity.[19] The interactions of SFT molecules with bacterial membrane structures have been suggested to induce various effects such as increasing its membrane permeability by channel formation and solubilization of cell membranes.[19] The cyclic heptapeptide head group of the SFT is a prerequisite for binding to the cell membranes after their primary collision.[19] The small-sized $SFT_{0.5}$/DT–Au NDs (2.20 nm) having a larger surface curvature enable a large amount of SFT assembled on the Au NDs. We determined that there are ≈150 SFT molecules per Au ND by ESI-Q-TOF MS. The Au NDs having high density of SFT ligands on its surfaces lead a strong multivalent interaction between SFT/DT–Au NDs and bacterial membranes.[30] Dehydration of the head groups of phospholipid, perturbation of lipid packing, and bilayer stability occur after SFT molecules enter bacteria membranes.[19] SEM images of *E. coli* exposed to SFT, DT–Au NDs, and $SFT_{0.5}$/DT–Au NDs for 1 h display varied morphological alteration (**Figure 3**A). On the other hand, the control cells had intact morphologies and smooth surfaces. Most of the *E. coli* treated with SFTs (500×10^{-6} M) or DT–Au NDs ([Au NDs] = 0.5×10^{-6} M) retained their intactness. In sharp contrast, a large number of cell debris were observed after treated with $SFT_{0.5}$/DT–Au NDs ([SFT] = 500×10^{-6} M, [Au NDs] = 0.5×10^{-6} M). The TEM image reveals that the $SFT_{0.5}$/DT–Au NDs at the surface of *E. coli* (Figure 3Bd). Energy-dispersive X-ray spectroscopy (EDS) measurements were conducted to further confirm the presence of the $SFT_{0.5}$/DT–Au NDs on the surface of *E. coli* (Figure 3C). Similarly, $SFT_{0.5}$/DT–Au NDs were also found at the surface of *S. aureus* and cause serious damage of the membrane of *S. aureus* (Figure S7, Supporting Information).

TEM images also reveal serious damage of the *E. coli* treated with $SFT_{0.5}$/DT–Au NDs, the obvious undulating appearance of a disorganized cell surface and blebs emanating from the cell membrane (Figure 3Bd). In comparison, the damage is less serious when they were treated with SFT or DT–Au NDs. This damage further results in disorganization of the cell membrane and cytoplasmic release. The disruption of *E. coli* by $SFT_{0.5}$/DT–Au NDs was also examined using SYTO 9 and PI to stain the nucleic acids. The green-fluorescent dye SYTO 9 was able to enter *E. coli*, but the red-fluorescent PI was excluded from

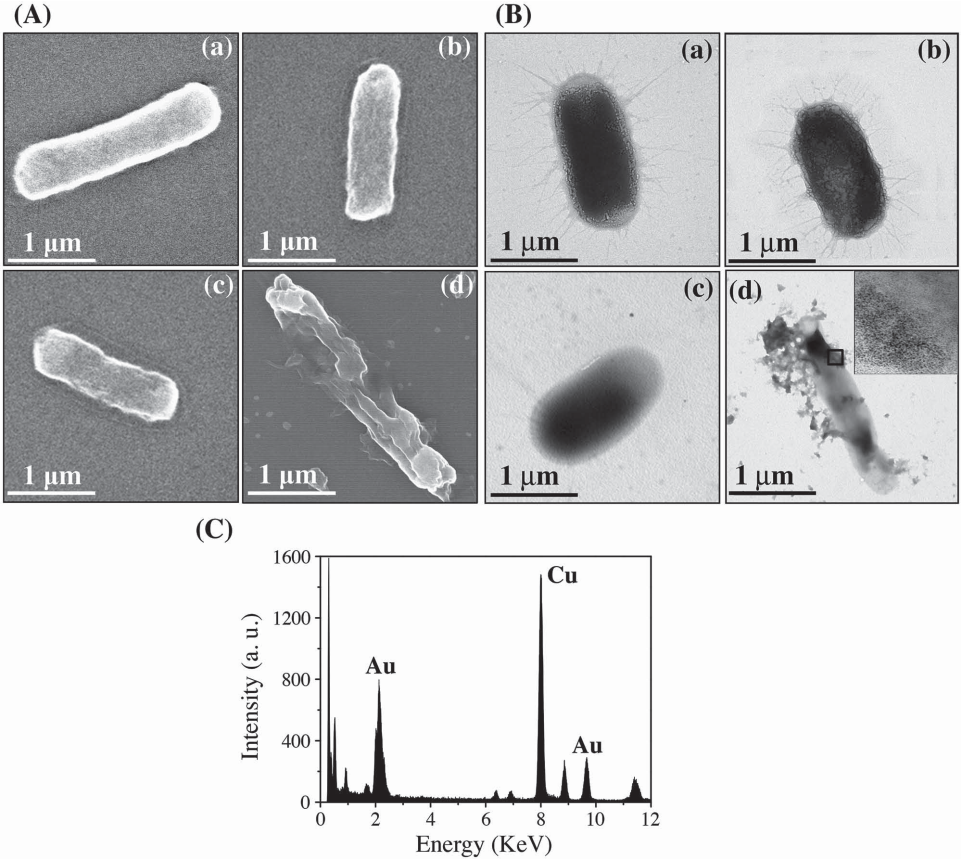

Figure 3. A) SEM and B) TEM images of a) *E. coli* cells and after treated with b) SFT solution (500×10^{-6} M), c) DT–Au NDs ([Au NDs] = 0.5×10^{-6} M), and d) $SFT_{0.5}$/DT–Au NDs ([SFT] = 500×10^{-6} M; [Au NDs] = 0.5×10^{-6} M). The inset to TEM image in (Bd): magnified view of the area enclosed with a solid line box indicating the presence of Au NDs at *E. coli*. C) TEM-EDS analysis of the magnified view of the area enclosed with a solid line box in TEM image (Bd). Other conditions were as described in Figure 2.

cells with structurally intact cytoplasmic membranes. The time-dependent fluorescence images of *E. coli* treated with $SFT_{0.5}$/DT–Au NDs (Figure S8, Supporting Information) clearly show serious damage to the cell membrane of *E. coli*. To further examine the disruption of bacteria, the activity of released β-galactosidase was determined using *o*-nitrophenyl-β-D-galactopyranoside (ONPG) substrates via measurement of absorption (at 420 nm) of the yellow product *o*-nitrophenol (ONP). As shown in Figure S9 (Supporting Information), the $SFT_{0.5}$/DT–Au NDs strongly induced the release of cytoplasmic β-galactosidase from *E. coli*. This result further supports our claim that the $SFT_{0.5}$/DT–Au NDs possess high antimicrobial activity, which destroyed the integrity of the bacterial membrane and caused the leakage of cytoplasm. The uptake of highly hydrophobic DT–Au NDs into the bacterial cell wall mediated by surface SFT ligands accelerated cell division, leading to disruption and lysis of the bacterial cells. In addition, multivalent SFT molecules on Au NDs might bind to proteins and/or peptidoglycans on the cell wall through hydrogen bonding and electrostatic interactions. These two factors resulted in synergistic damage of the cell wall and/or inhibition of cell wall synthesis. The destruction of fimbriae was observed from $SFT_{0.5}$/DT–Au NDs-treated *E. coli* (Figure 3Bd), supporting the claim of serious damage to the integrity of the cell membrane caused by $SFT_{0.5}$/DT–Au NDs.

Bacterial resistance is generally rare against cyclic lipopeptides due to their nonspecific disruption of cell membranes.[31] Only very few bacteria strains (e.g., *Streptomyces sp*. Mg1) was resistant to inhibition by surfactin.[32] The complex permeabilization to bacterial membranes induced by surfactin leads it to be able to disrupt all types of bacterial cell membranes, bearing on its tendency to not produce resistant strains of bacteria. The bacteria strains used in this study were not resistant to the inhibition by surfactin.[33] Therefore, high antibacterial SFT/DT–Au NDs are unlikely to trigger bacterial resistance of used bacteria in this study. However, the antibacterial activity of SFT/DT–Au NDs against surfactin-resistant bacteria strain will be investigated in the future.

2.4. Cytotoxicity and Hemolysis Evaluation

Two major side effects caused by antimicrobial peptides are hemolysis and cytotoxicity toward mammalian cells and RBCs, respectively.[34] The cytotoxicity of $SFT_{0.5}$/DT–Au NDs toward mammalian cells was evaluated using an Alamar Blue assay. After 24 h of separated incubation of MCF-10A, NIH-3T3, and HMEC-1 cells with the $SFT_{0.5}$/DT–Au NDs at concentration $< 1000 \times 10^{-6}$ M (in terms of the concentration of SFT), the cell viability values were all higher than 90% (Figure S10B, Supporting Information), which are 300-fold higher than MIC for tested bacteria (Figure 2). The biocompatibility of $SFT_{0.5}$/DT–Au NDs toward the tested mammalian cells was superior to free SFT at the same concentration. Our results suggest the cytotoxicity of SFT promptly decreased after being loaded onto the surface of Au NDs, mainly due to weaker interaction of the SFT with the mammalian cell membranes. Compared to bacterial membranes, mammalian cell membranes are composed principally of lipids with less net charge and are rich in cholesterol. Therefore, the excellent selectivity of $SFT_{0.5}$/DT–Au NDs toward bacteria is mainly ascribed to the differences in membrane properties of bacterial and mammalian cells.

In addition, satisfactory biocompatibility was verified by a hemolysis test. Hemolytic evaluations were conducted using human RBCs incubated with $SFT_{0.5}$/DT–Au NDs or SFT at various concentrations (Figure S11, Supporting Information). Compared with SFT at the same concentration, significantly less hemolysis of RBCs caused by $SFT_{0.5}$/DT–Au NDs was observed. For example, at 500×10^{-6} M, a concentration much lower than the MIC, almost no hemolysis was observed with the $SFT_{0.5}$/DT–Au NDs, whereas free SFT caused more than 95% hemolysis. Preferential toxicity to bacterial cells and insignificant cytotoxicity to the mammalian cells and hemolytic effect to RBC insinuate the emergence of SFT/DT–Au NDs as a potential antimicrobial drug.

2.5. Wound Healing Activity

To demonstrate the practical applicability of the SFT/DT–Au NDs, we tested its antibacterial ability in healing of skin wounds of rats exposed to MRSA. **Figure 4**A shows photographs of postoperative wound healing in SD rats that had (not) been subjected to treatment with SFT or SFT/DT–Au NDs. Figure 4B shows the graphical representation of the quantitative measurement of the wound area. As can be seen from Figure 4A, wound crust started appearing at the $SFT_{0.5}$/DT–Au NDs dressed wound site on the 6th d postsurgery and an ≈60% decrease in the wound size was observed (Figure 4B), thereby showing effective healing. Even though the other two groups, untreated and SFT, also showed signs of wound closure (decreased to ≈75% and ≈60%, respectively), the wound crust did not appear on the 6th d. Also, ulceration and edema were seen on the untreated wound site even after 6 d, showing poor inhibition of the bacterial infection. By day 9 we observed significantly greater epithelial coverage in the $SFT_{0.5}$/DT–Au NDs group and only ≈5% wound crust was observed. The 12th d postsurgery shows complete re-epithelialization of wounds treated with $SFT_{0.5}$/DT–Au NDs, exhibiting thicker granulation tissue and more extensive development of hair follicles when compared with that of the control group and SFT group. To check the antibacterial activity, the bacteria from the tissues in the wound area were cultured on agar plates overnight (Figure 4C). Since no antibacterial agent was applied, the 2nd d samples showed high bacterial growth for all groups. On the 4th d, culture from the $SFT_{0.5}$/DT–Au NDs group showed very significant decrease in bacterial count. By contrast, the SFT group showed a little decrease, while untreated group did not show any change. Moreover, relative to $SFT_{0.5}$/DT–Au ND treated wound, the wound of the control group and SFT group excreted exudate continuously, which prolonged the healing process. After 9 d postsurgery, SFT and $SFT_{0.5}$/DT–Au NDs groups showed complete recovery from bacterial infection. Consistent with the in vitro antibacterial assay, $SFT_{0.5}$/DT–Au ND shows better bacteria membrane rupture through a variety of mechanisms.[19] Thus, $SFT_{0.5}$/DT–Au NDs are a better antibacterial agent than only SFT.

Histological analysis in the infected full-thickness wounds was also performed by hematoxylin and eosin (H&E) staining

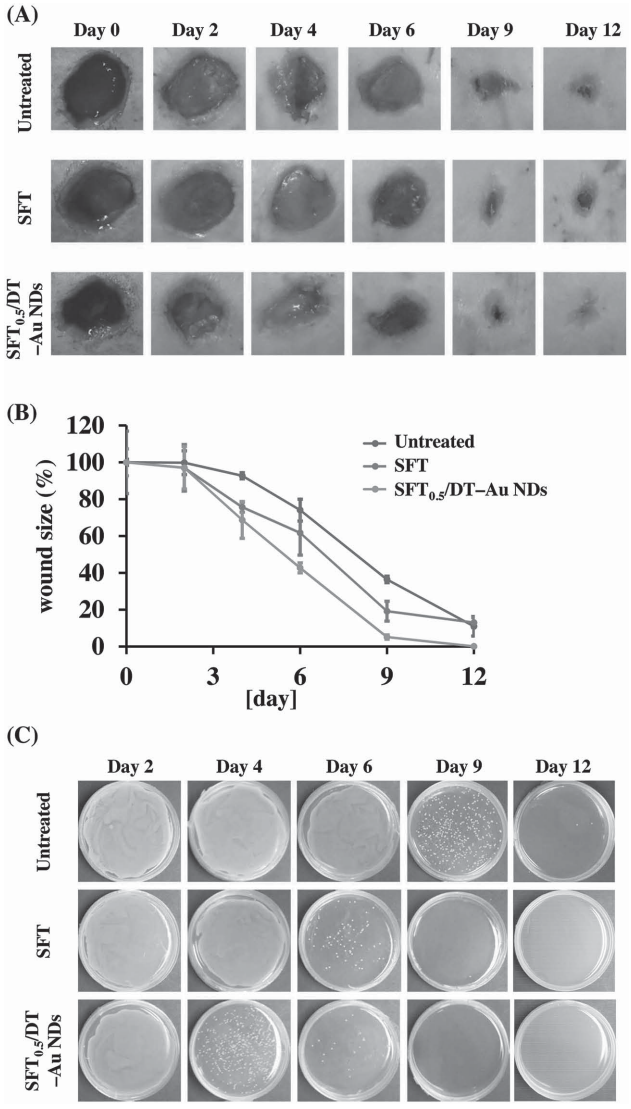

Figure 4. A) Representative photographs of the MRSA-infected wound untreated and treated with SFT or SFT/DT–Au NDs and B) their corresponding wound sizes (relative area versus initial area). Error bars represent the standard deviation of three repeated measurements. C) Photographs of bacterial cultures from the tissue of untreated, and SFT or SFT/DT–Au NDs treated wound.

to compare the untreated wounds with the $SFT_{0.5}$/DT–Au NDs-treated wounds (**Figure 5**A). Clear distinction of the boundary between the normal and wound tissue can be seen on day 2 (indicated by a green line). The epithelial tissue due to the migration of keratinocytes from the surrounding tissue to the wound bed was apparent (indicated by a red arrow) at the wound margin in $SFT_{0.5}$/DT–Au NDs-treated wound on day 4. On day 6, the untreated group showed some migration of keratinocytes from the normal tissue area to the wound sites (indicated by a black arrow), but the boundary between them is distinguishable and only a little healing was observed. However, a greater migration for keratinocytes and a better healing was observed for the $SFT_{0.5}$/DT–Au NDs treated wound. On day 9, the skin morphology was close to normal healthy epidermis and exhibited an adequate thickness of the epidermal layer, whereas the dermal layer in the untreated group was not yet fully regenerated (indicated by a blue arrow). More blood vessels (indicated by purple arrows) and hair follicles (indicated by cyan arrows) developed in the $SFT_{0.5}$/DT–Au ND treated wound site, and the wound crust disappeared on day 12; moreover, it looked identical to that of normal tissue. Conversely, no hair follicles or blood vessels developed at the untreated wound sites after 12 d, even though the wound curst was present (indicated by an yellow arrow).

Masson's trichrome staining was used to visualize the formation and distribution of collagen during the healing process of the wounded tissues (Figure 5B). The collagen fibers were stained blue, and the intensity represents the relative collagen content in the tissue sections. The wound sites show significantly less collagen fibers deposition compared with the adjacent normal tissue on the 2nd d postsurgery. On the 4th d postsurgery, the $SFT_{0.5}$/DT–Au ND treated group showed a higher density of collagen fibers (deeper blue color) when compared to the untreated group. On the 6th d, when compared to the untreated wound site, the $SFT_{0.5}$/DT–Au ND treated wound site contained dense collagen fibers and increasing neovascularization formation (indicated by red arrows). On day 9, the neovascularization (indicated by red arrows) and the formation of new collagen fibers were significantly more prominent at the $SFT_{0.5}$/DT–Au ND treated wound site, contributing to a faster and better wound healing process. Moreover, significant collagen content did not appear until day 9 at the untreated wound site. On day 12, the wound of the $SFT_{0.5}$/DT–Au ND treated group was completely healed, showing an identical distribution of collagen and blood vessels with the normal tissues, while the untreated wound site displayed little increase in collagen content and blood vessel number than those on the 6th and 9th d. In general, we observed higher collagen content in the $SFT_{0.5}$/DT–Au ND treated wound site from day 4 to day 12 postsurgery compared with that of the untreated wound. Therefore, higher fibroblast formation and collagen secretion presumably accelerated the wound healing process. Our results suggest that the nanostructure feature of $SFT_{0.5}$/DT–Au NDs modulates the collagen alignment to improve the mechanical properties in wound healing.[35]

3. Conclusions

We have demonstrated that the antibacterial peptide formed a dense shell on each core of photoluminescent Au NDs through self-assembly. The density of SFT on Au NPs has a significant effect on determining the size and photoluminescent QY of SFT/DT–Au NDs, as well as their antibacterial potency. Relative to free SFT, SFT/DT–Au NDs exhibited much higher antibacterial activity to MRSA due to their strong effect on disintegration of the bacterial membrane. The cytotoxicity and hemolysis assays and bacterial wound healing studies have revealed SFT/DT–Au NDs are an attractive biocompatible nanocomposite for topical applications in the treatment of wounds. Recently, glutathione (GSH)-, dihydrolipoic acid (DHLA)-, or cyclodextrin (CD)-capped silver nanoclusters (Ag NCs) have demonstrated strong antimicrobial activity due to abundant Ag^+ ions

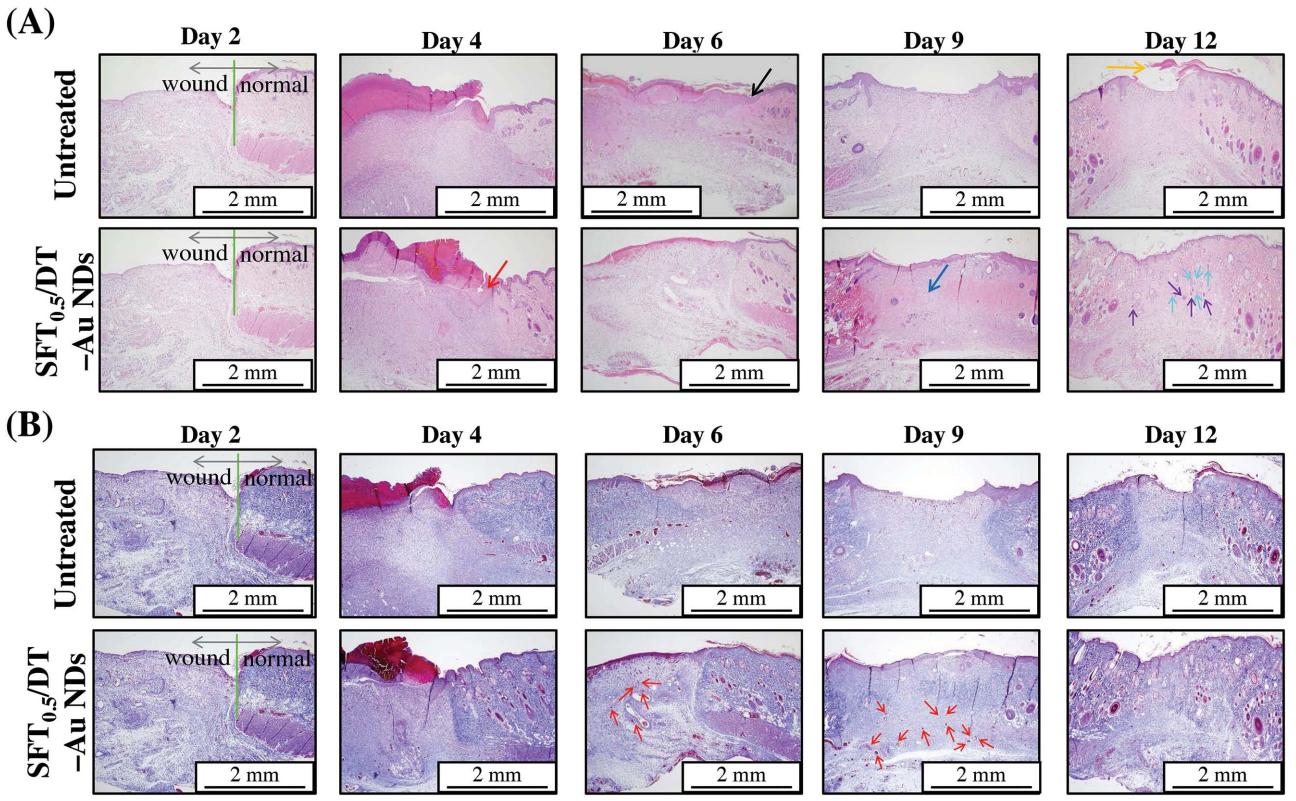

Figure 5. Histologic analysis of wound tissue using A) hematoxylin and eosin and B) Masson's trichrome staining.

on Ag NCs surfaces and high capability to generation of the ROS.[36] In contrast, the mainly antimicrobial effect of our SFT/DT–Au NDs is through disruption of the integrity of the bacterial membrane, leading to the leakage of cytoplasm. Therefore, the assembly of SFT/DT to silver NDs or alloy gold/silver NDs to form SFT/DT–Ag NDs or SFT/DT–Au/Ag NDs is expected to further improve the antibacterial activity of NDs.

4. Experimental Section

Chemicals: Tetrachloroauric acid trihydrate ($HAuCl_4{\cdot}3H_2O$), DT, THPC, ONPG, acetonitrile (ACN), and aqueous formic acid (FA) solution (8% in water) were purchased from Sigma-Aldrich (Milwaukee, WI, USA). Tris(hydroxymethyl)aminomethane (Tris), potassium chloride, magnesium chloride, phosphoric acid, and trisodium phosphate were purchased from J. T. Baker (Phillipsburg, NJ, USA). The sodium phosphate buffer (pH 7.4, 100×10^{-3} M) was prepared with phosphoric acid (100×10^{-3} M) and trisodium phosphate (100×10^{-3} M). Fetal bovine serum (FBS) and all cell culture media were purchased from Gibco BRL (Grand Island, NY, USA). Antibiotic–antimycotic, L-glutamine, and nonessential amino acids were obtained from Biowest (Lewes, UK). Alamar Blue reagent was purchased from BioSource (Camarillo, CA, USA). The SYTO Green-Fluorescent Nucleic Acid Stains assay kit was purchased from Molecular Probes (Eugene, Oregon, USA). B-PER bacterial protein extraction reagent (bacteria lysis agent) was purchased from Thermo Fisher Scientific Inc. (Rockford, IL, USA). Surfactin from *Bacillus subtilis* (≥98%, HPLC grade) was provided by Prof. Lu (Department of Aquaculture, National Taiwan Ocean University).

Synthesis and Characterization of Photoluminescent SFT/DT–Au NDs: Non photoluminescent Au NPs (diameter ≈3.2 nm; $\approx 1.0 \times 10^{-6}$ M) were synthesized by THPC (1.5×10^{-3} M)-mediated reduction of $HAuCl_4$ (840×10^{-6} M).[21] For preparation of photoluminescent SFT/DT–Au NDs, aliquots of the as-prepared Au NPs (0.5×10^{-6} M) were self-assembled with DT (1.0×10^{-3} M) and SFT ($0–1.0 \times 10^{-3}$ M) in trisodium tetraborate buffer solution (20×10^{-3} M, pH 9.2) for 48 h at ambient temperature. The photoluminescence and UV–vis absorption spectra of the as-prepared DT–Au NDs and SFT/DT–Au NDs were recorded using a spectrofluorometer (Cary Eclipse; Varian, Walnut Creek, CA, USA) and a double beam UV–vis spectrophotometer (Cintra 10e, GBC, Victoria, Australia), respectively. For the determination of quantum yield (Φ_f) values of the DT–Au NDs and SFT/DT–Au NDs, each of their diluted solution (100×10^{-9} M, 0.50 mL) was placed in a quartz cuvette (1 cm path length of light). The Φ_f values were determined by comparison with that of 10^{-6} M quinine (Φ_f = 53%, in 0.10 M H_2SO_4). The average size of the Au NPs and Au NDs was determined using a transmission electron microscope (Tecnai 20 G2 S-Twin TEM, Philips/FEI, Hillsboro, Oregon, USA), with each of the purified samples deposited onto a TEM grid with a thin layer of carbon. X-ray photoelectron spectroscopy (XPS) measurements of the SFT/DT–Au NDs were performed using an ES-CALAB 250 spectrometer (VG Scientific, East Grinstead, UK) with Al Kα X-ray radiation as the X-ray source for excitation. Their binding energies were corrected using the C 1s peak at 284.6 eV as a standard. The samples for XPS measurements were prepared by depositing drops of the DT–Au NDs or SFT/DT–Au NDs onto Si substrates, in which the solvents evaporated at ambient temperature and pressure. The photoluminescence lifetimes of the DT–Au NDs and SFT/DT–Au NDs were recorded using a photo-counting PicoHarp 300 system (PicoPicoQuant, Berlin, Germany) and a diode laser emitting at 375 nm (FluoTime 300) as the light source. The $SFT_{0.5}$/DT–Au NDs was stable (no aggregation formed) in phosphate-buffered saline (PBS) and bacteria culture medium for at least 48 h. The intensities of static light scattering of $SFT_{0.5}$/DT–Au NDs (500×10^{-9} M) in 5×10^{-3} M sodium phosphate, PBS, or bacteria culture medium were determined to be close (320 ± 45 kcps, $n = 3$) by using a particle size analyzer (Zetasizer Nano, Malvern, Orcestershire, UK).

ESI-Q-TOF MS Measurements: The SFT/DT–Au NDs were purified through centrifugal filtration at a relative centrifugal force (RCF) of 13 500 *g* for 20 min using a filter having a cutoff of 50 kDa and then washing twice with deionized (DI) water. SFT solution (100×10^{-6} M) and purified SFT/DT–Au NDs (1.0×10^{-6} M) were analyzed using an ESI-Q-TOF MS (Waters SYNAPT G2 HDMS, Waters Corp., Milford, MA, USA). A 15 µL aliquot of SFT solution or purified SFT/DT–Au NDs was mixed with 5.0 µL of 40% methanol solution, and analyzed by ESI-Q-TOF MS. Each of the mixtures was injected into a 180 µm (i.d.) × 2.0 cm capillary trap column. ESI-Q-TOF MS was operated with a spray voltage of 3.0 kV. NanoLockSpray source was used for accurate mass measurement, and the lock mass channel was sampled every 30 s. Data acquisition was operated in data direct analysis (DDA) mode. The DDA method included one full MS scan (*m*/*z* 200–2000 for 1.0 s) sequentially on the three most intense ions present in the full-scan mass spectrum. Each sample was analyzed in triplicate.

Bacterial Cultures: Five strains of *S. aureus*, *S. enteritidis*, MRSA, *E. coli*, and *P. vulgaris* were obtained from the Institute of Food Science (Hsinchu, Taiwan). All bacteria were grown separately in sterile Luria–Bertani (LB) media [containing bacto-tryptone (2.5 g), bacto-yeast extract (1.25 g), and NaCl (1.25 g) in 250 mL of deionized water]. A single colony of each strain was lifted from LB agar plates and inoculated in LB media (10 mL). The cultures were grown at 37 °C with orbital shaking [200 revolutions per minute (rpm)] until the value of the absorption at 600 nm (OD_{600}) reached 1.0. Each of the cell mixtures (1.0 mL) was centrifuged (RCF 3500 *g*, 10 min, 25 °C) and washed twice with PBS (pH 7.4, containing 137×10^{-3} M NaCl, 2.7×10^{-3} M KCl, 10×10^{-3} M Na_2HPO_4, and 2.0×10^{-3} M KH_2PO_4) solution for further use. Bacterial cell suspensions were diluted to obtain cell samples containing 10^4–10^5 colony-forming units (CFU) per milliliter.

Antimicrobial Activity: The MICs of SFT, DT–Au NDs, and SFT/DT–Au NDs against different bacterial strains were determined using the broth microdilution method. *S. aureus*, *S. enteritidis*, MRSA, *E. coli*, and *P. vulgaris* cells (each 1.0×10^3 cells mL^{-1}) were incubated separately with SFTs ($0.001–10 \times 10^{-3}$ M), DT–Au NDs ([Au NDs] = $0.002–2.0 \times 10^{-6}$ M) or SFT/DT–Au NDs ([SFT] = $0.0011.0 \times 10^{-3}$ M) that were dissolved/dispersed in sodium phosphate solutions (5.0×10^{-3} M, pH 7.4) at 37 °C under orbital shaking at a speed of 250 rpm for 2 h. Cultures were then grown in LB media at 37 °C with orbital shaking (200 rpm) for 16 h. Negative controls were conducted in wells that contained only broth or inoculated broth. The bacterial cultures were then serially diluted 10^7-fold and the cell densities were determined by CFU count on LB agar plates. The inhibitory effect was calculated using the formula: percent inhibition = $(1 - T/C) \times 100\%$, where *T* and *C* (CFU mL^{-1}) are cell densities of the test and control samples, respectively. Each experiment was performed in duplicate and repeated thrice. The MIC values were reported as the lowest concentration of SFT or SFT/DT–Au NDs capable of completely inhibiting the growth of each bacterial strain tested.

Zone of Inhibition: The SFT (500×10^{-6} M, 100 µL), DT–Au NDs ([Au NDs] = 0.5×10^{-6} M, 100 µL), or SFT/DT–Au NDs ([SFT]/[DT] = $500/1000 \times 10^{-6}$ M; [Au NDs] = 0.5×10^{-6} M, 100 µL)-loaded paper discs (diameter: 0.8 cm; 100% alpha cotton cellulose, ADVANTEC, Toyo Roshi Kaisha, Ltd., Japan) were prepared by dropping the antimicrobial solutions onto filter paper discs separately. A well-diffusion method was used to determine their antimicrobial activities against test strains on LB agar. A total of 100 µL of diluted inoculum (1.0×10^9 CFU mL^{-1}) from *E. coli* or *S. aureus* suspension was spread on the surface of the plates to solidify. The paper discs were then placed onto each plate. After incubation overnight at 37 °C, the sizes of the zones of inhibition were measured. Unmodified paper discs were used as a negative control.

Fluorescence Staining and TEM Images: The bacterial suspensions of *E. coli* (≈10^9 CFU mL^{-1}, 1.0 mL) were centrifuged (3500 *g*, 10 min, 25 °C) and washed twice with 5.0×10^{-3} M phosphate buffer solution (pH 7.4). Aliquots (50 µL) of *E. coli* suspension (1.0×10^9 CFU mL^{-1}) were incubated with the SFT/DT–Au NDs ([SFT]/[DT] = $500/1000 \times 10^{-6}$ M; [Au NDs] = 0.5×10^{-6} M) in 5.0×10^{-3} M sodium phosphate solution (pH 7.4) for 10 min or 1 h, which were then purified (RCF 3500 *g* for 10 min) and washed with 5.0×10^{-3} M sodium phosphate solution (pH 7.4; 1.0 mL × 3) to remove the matrix. The fluorescence images of the treated bacteria were captured using an Olympus BX61 microscope (Tokyo, Japan) with a DP71 digital camera. The fluorescence image of Au NDs-captured bacteria (excitation wavelength, 380 nm; emission wavelength, 510 nm) was recorded. Prior to TEM measurements, drops of the Au NDs-captured bacteria solution were carefully deposited onto 400-mesh copper-coated grids. The TEM-EDS analysis of these treated bacteria samples were captured using a TEM equipped with an EDS.

Permeabilization Assay: The permeabilization of bacteria membranes was assessed by determining the enzymatic activity of released β-galactosidase using an ONPG substrate. A positive control of lysis solution of *E. coli* (500 µL) was accomplished by B-PER performed at 37 °C with orbital shaking (200 rpm) for 2 h. The supernatants (450 µL) (centrifuged at RCF of 3500 *g* for 10 min) of Au NDs-treated *E. coli* solutions and the lysed *E. coli* solution were separately diluted tenfold with PBS solution, which were then reacted with ONPG substrate solutions (1.0×10^{-3} M, 50 µL) at ambient temperature for 2 h. The mixtures were then transferred separately into 96-well microtiter plates, and their absorption spectra were recorded using a Synergy 4 microplate spectrophotometer at a wavelength of 420 nm.

Cell Culture and Cytotoxicity Assays: MCF-10A, NIH-3T3, and HMEC-1 were obtained from the American Type Culture Collection (ATCC; Manassas, VA, USA). MCF-10A cells were cultured in α-MEM supplemented with prequalified human recombinant EGF 1–53, bovine pituitary extract, FBS (10%), and antibiotic–antimycotic (1.0%). NIH-3T3 cells were maintained in DMEM supplemented with FBS (10%), antibiotic–antimycotic (1.0%), L-glutamine (2.0×10^{-3} M), and nonessential amino acids (1.0%). HMEC-1 cells were cultured in MCDB 131 medium supplemented with FBS (10%), antibiotic–antimycotic (1.0%), L-glutamine (2.0×10^{-3} M), epithelial growth factor (10 ng mL^{-1}), and hydrocortisone (1.0 µg mL^{-1}). The cell number and viability of the cells were determined by applying the trypan blue exclusion method and Alamar Blue assay, respectively. Following the separated incubation of MCF-10A, NIH-3T3, and HMEC-1 cells (≈10^4 cells per well) in a culture medium for 24 h at 37 °C containing 5% CO_2, each of the culture media was replaced with 100 µL of cell culture medium containing SFT ($0–1.0 \times 10^{-3}$ M) or SFT/DT–Au NDs ([SFT] = $0–1.0 \times 10^{-3}$ M) and then further cultured for an additional 48 h. The cells were carefully rinsed thrice with PBS solution and then reacted with Alamar Blue reagent for 2 h. Fluorescence of the as-formed reduced dye was measured using a Synergy 4 microplate spectrophotometer, with an excitation wavelength of 545 nm and an emission wavelength of 590 nm. Because fluorescence intensity is directly correlated with cell quantity, cell viability was calculated by assuming 100% viability in the control set (media without SFT and SFT/DT–Au NDs).

Hemolysis Assays: Hemolysis induced by SFT and SFT/DT–Au NDs was tested according to a previous report.[37] Fresh blood samples from a healthy volunteer (25 years old) were drawn from the vein into tubes containing EDTA, which were immediately (within 30 min of collection) centrifuged (RCF 3000 *g*, 10 min, 4 °C) to remove serum. Fresh RBCs were then washed thrice with sterile isotonic PBS. Following the last wash, the RBCs were diluted with sterile isotonic PBS to obtain an RBC stock suspension (4.0 vol% blood cells). The RBC stock suspension (200 µL) was added to each of the SFT ($0–1.0 \times 10^{-3}$ M) or SFT/DT–Au NDs ([SFT] = $0–1.0 \times 10^{-3}$ M) solutions in 1.5 mL vials, respectively. After 1 h of incubation at 37 °C, the mixtures were centrifuged separately at RCF of 1000 *g* for 10 min. Hemoglobin absorption at 576 nm ($OD_{576\ sample}$) of each supernatant (150 µL) was recorded separately. Hemolysis activity was then determined according to the following formula

$$\text{Hemolysis}(\%) = \left[\left(OD_{576\ sample} - OD_{576\ blank}\right) / \left(OD_{576\ ultrapure\ water} - OD_{576\ blank}\right)\right] \times 100 \quad (1)$$

Sterile isotonic PBS ($OD_{576\ blank}$) was used as a reference for 0% hemolysis, while the absorbance ($OD_{576\ ultrapure\ water}$) of the solution prepared by adding ultrapure water to the RBC stock suspension was set as 100% hemolysis.

Wound Healing: The wound healing efficacy of the SFT/DT–Au NDs was evaluated using a rat model with slight modification to a reported

procedure.[38] Permission for the rat animal study was obtained from the Institutional Animal Care and Use Committee of the National Laboratory Animal Center (NLAC; Permit No. IACUC2012-037). Sprague Dawley (SD) male rats weighing ≈250 g were anesthetized with Zoletil with a dose of 50 mg kg^{-1} of body weight. The dorsum skin of the rat was shaved, and then disinfected using 70% ethanol for aseptic surgery. Circular skin wounds with a diameter of 1 cm were made by incision of the dorsum of each rat with a stainless steel scissor and the skin was removed. Then, MRSA suspension (100 µL) containing 1×10^8 CFU in presterilized saline was placed on the wound site, which was then covered with a sterilized cotton gauze moistened with PBS to keep the bacteria growing. After 2 d postsurgery, the wound area was sampled using a sterile swab and it was plated in the LB agar and left to incubate for 8 h at 37 °C to confirm MRSA infection. Similarly, the samples were taken after 4, 6, 9, and 12 d and cultured to check the antibacterial activity. The dressing was prepared by dipping SFT/DT–Au NDs ([SFT] = 100×10^{-6} M; 200 µL) or SFT ([SFT] = 100×10^{-6} M; 200 µL) in gauze (1.5 cm × 1.5 cm). Then the wounded areas were covered with SFT/DT–Au NDs/gauze or SFT/gauze, each of which was fixed with an elastic adhesive bandage. Control wounds were just covered with gauze without any drug loading, as an untreated control. Wound closure observation of each rat was assessed by a digital camera on days 2, 4, 6, 9, and 12 postwounding surgery. The wound closure rate is expressed by the following equation

$$\text{Wound size}\,(\%) = \left(A_o - A_t\right)/A_o \times 100 \quad (2)$$

where A_o is the original wound area and A_t is the wound area at specified time point.

For histology, the skin, including the entire wound with adjacent normal skin, was excised and fixed with 10% formaldehyde solution. The specimen included the dermis and subcutaneous tissue. The tissue samples were analyzed by H&E staining for histological testing, and also by Masson's trichrome staining for examining the formation of collagen.

Supporting Information

Supporting Information is available from the Wiley Online Library or from the author.

Acknowledgements

W.-Y.C. and H.-Y.C. contributed equally to this work. This study was supported by the Ministry of Science and Technology of Taiwan under Contract Nos. 104-2628-M-019-001-MY3, 103-2627-M-007-002-MY3, and 102-2113-M-019-001-MY3. The assistance of Ms. Ya-Yun Yang and Ms. Ching-Yen Lin from the Instrument Center of National Taiwan University (NTU) for TEM and SEM measurements is appreciated. Thanking Ms. Corina Leung from the Mass Spectrometry-based Proteomic Core Facility in National Taiwan University for assistance with the ESI-MS measurements.

Received: August 4, 2015
Revised: September 12, 2015
Published online: October 23, 2015

[1] a) L. Diacovich, J.-P. Gorvel, *Nat. Rev. Microbiol.* **2010**, *8*, 117; b) R. E. W. Hancock, A. Nijnik, D. J. Philpott, *Nat. Rev. Microbiol.* **2012**, *10*, 243; c) J. G. Hurdle, A. J. O'Neill, I. Chopra, R. E. Lee, *Nat. Rev. Microbiol.* **2011**, *9*, 62.

[2] M. A. Kohanski, D. J. Dwyer, J. J. Collins, *Nat. Rev. Microbiol.* **2010**, *8*, 423.

[3] a) P. J. Bergen, C. B. Landersdorfer, H. J. Lee, J. Li, R. L. Nation, *Curr. Opin. Infect. Dis.* **2012**, *25*, 626; b) Z.-Q. Xu, M. T. Flavin, J. Flavin, *Expert Opin. Invest. Drugs* **2014**, *23*, 163; c) N. Woodford, J. F. Turton, D. M. Livermore, *FEMS Microbiol. Rev.* **2011**, *35*, 736; d) E. M. H. Wellington, A. B. A. Boxall, P. Cross, E. J. Feil, W. H. Gaze, P. M. Hawkey, A. S. Johnson-Rollings, D. L. Jones, N. M. Lee, W. Otten, C. M. Thomas, A. P. Williams, *Lancet Infect. Dis.* **2013**, *13*, 155.

[4] a) M. Hassan, M. Kjos, I. F. Nes, D. B. Diep, F. Lotfipour, *J. Appl. Microbiol.* **2012**, *113*, 723; b) S.-C. Park, Y. Park, K.-S. Hahm, *Int. J. Mol. Sci.* **2011**, *12*, 5971.

[5] a) A. A. Bahar, D. Ren, *Pharmaceuticals* **2013**, *6*, 1543; b) J. Cruz, C. Ortiz, F. Guzmán, R. Fernández-Lafuente, R. Torres, *Curr. Med. Chem.* **2014**, *21*, 2299; c) G. Wang, *Pharmaceuticals* **2014**, *7*, 545; d) A. L. Hilchie, K. Wuerth, R. E. W. Hancock, *Nat. Chem. Biol.* **2013**, *9*, 761; e) Y. Li, Q. Xiang, Q. Zhang, Y. Huang, Z. Su, *Peptides* **2012**, *37*, 207.

[6] a) M. UlIslam, A. Shehzad, S. Khan, W. A. Khattak, M. W. Ullahl, J. K. Park, *J. Nanosci. Nanotechnol.* **2014**, *14*, 780; b) F. Hossain, O. J. Perales-Perez, S. Hwang, F. Román, *Sci. Total Environ.* **2014**, *466*, 1047; c) Q. Li, S. Mahendra, D. Y. Lyon, L. Brunet, M. V. Liga, D. Li, P. J. J. Alvarez, *Water Res.* **2008**, *42*, 4591.

[7] a) T. N. V. K. V. Prasad, V. S. R. Kambala, R. Naidu, *Curr. Nanosci.* **2011**, *7*, 531; b) S. M. Dizaj, F. Lotfipour, M. Barzegar-Jalali, M. H. Zarrintan, K. Adibkia, *Mater. Sci. Eng., C* **2014**, *44*, 278; c) M. Rai, A. Yadav, A. Gade, *Biotechnol. Adv.* **2009**, *27*, 76; d) P. J. P. Espitia, N. de F. F. Soares, J. S. dos R. Coimbra, N. J. de Andrade, R. S. Cruz, E. A. A. Medeiros, *Food Bioprocess Technol.* **2012**, *5*, 1447.

[8] a) M. Ishihara, V. Q. Nguyen, Y. Mori, S. Nakamura, H. Hattori, *Int. J. Mol. Sci.* **2015**, *16*, 13973; b) A. Herman, A. P. Herman, *J. Nanosci. Nanotechnol.* **2014**, *14*, 946.

[9] A. M. Allahverdiyev, E. S. Abamor, M. Bagirova, M. Rafailovich, *Future Microbiol.* **2011**, *6*, 933.

[10] a) S. J. Soenen, W. J. Parak, J. Rejman, B. Manshian, *Chem. Rev.* **2015**, *115*, 2109; b) A. P. Ingle, N. Duran, M. Rai, *Appl. Microbiol. Biotechnol.* **2014**, *98*, 1001; c) I. M. Adjei, B. Sharma, V. Labhasetwar, *Adv. Exp. Med. Biol.* **2014**, *811*, 73; d) E. Fröhlich, *Int. J. Nanomed.* **2012**, *7*, 5577.

[11] a) A. M. Allahverdiyev, K. V. Kon, E. S. Abamor, M. Bagirova, M. Rafailovich, *Expert Rev. Anti-Infect. Ther.* **2011**, *9*, 1035; b) L. Zhang, D. Pornpattananangkul, C. M. J. Hu, C. M. Huang, *Curr. Med. Chem.* **2010**, *17*, 585; c) H. Sun, N. Gao, K. Dong, J. Ren, X. Qu, *ACS Nano* **2014**, *8*, 6202; d) M. Yin, Z. Li, E. Ju, Z. Wang, K. Dong, J. Ren, X. Qu, *Chem. Commun.* **2014**, *50*, 10488.

[12] a) M. Grzelczak, J. Vermant, E. M. Furst, L. M. Liz-Marzán, *ACS Nano* **2010**, *4*, 3591; b) M. G. Moffitt, *J. Phys. Chem. Lett.* **2013**, *4*, 3654.

[13] a) Y.-C. Shiang, C.-C. Huang, T.-H. Wang, C.-W. Chien, H.-T. Chang, *Adv. Funct. Mater.* **2010**, *20*, 3175; b) H. Zhang, F. Li, B. Dever, C. Wang, X.-F. Li, X. C. Le, *Angew. Chem. Int. Ed.* **2013**, *52*, 10698.

[14] a) I. Fratoddi, I. Venditti, C. Cametti, M. V. Russo, *J. Mater. Chem. B* **2014**, *2*, 4204; b) A. Kumar, X. Zhang, X.-J. Liang, *Biotechnol. Adv.* **2013**, *31*, 593; c) R. V. Devi, M. Doble, R. S. Verma, *Biosens. Bioelectron.* **2015**, *68*, 688.

[15] a) A. Rai, A. Prabhune, C. C. Perry, *J. Mater. Chem.* **2010**, *20*, 6789; b) M. M. R. Mollick, B. Bhowmick, D. Mondal, D. Maity, D. Rana, S. K. Dash, S. Chattopadhyay, S. Roy, J. Sarkar, K. Acharya, M. Chakraborty, D. Chattopadhyay, *RSC Adv.* **2014**, *4*, 37838; c) Y. Tao, E. Ju, J. Ren, X. Qu, *Adv. Mater.* **2015**, *27*, 1097; d) T. Ahmad, I. A. Wani, N. Manzoor, J. Ahmed, A. M. Asiri, *Colloids Surf., B* **2013**, *107*, 227; e) W.-Y. Chen, J.-Y. Lin, W.-J. Chen, L. Luo, E. W.-G. Diau, Y.-C. Chen, *Nanomedicine* **2010**, *5*, 755; f) X. Li, S. M. Robinson, A. Gupta, K. Saha, Z. Jiang, D. F. Moyano, A. Sahar, M. A. Riley, V. M. Rotello, *ACS Nano* **2014**, *8*, 10682.

[16] C.-C. Huang, Z. Yang, K.-H. Lee, H.-T. Chang, *Angew. Chem. Int. Ed.* **2007**, *46*, 6824.

[17] N. S. Shaligram, R. S. Singhal, *Food Technol. Biotechnol.* **2010**, *48*, 119.
[18] G. Seydlová, J. Svobodová, *Cent. Eur. J. Med.* **2008**, *3*, 123.
[19] a) H. Heerklotz, J. Seelig, *Biophys. J.* **2001**, *81*, 1547; b) M. Deleu, J. Lorent, L. Lins, R. Brasseur, N. Braun, K. El Kirat, T. Nyçlander, Y. F. Dufrêne, M.-P. Mingeot-Leclercq, *Biochim. Biophys. Acta* **2013**, *1828*, 801; c) H. Heerklotz, J. Seelig, *Eur. Biophys. J.* **2007**, *36*, 305; d) C. Carrillo, J. A. Teruel, F. J. Aranda, A. Ortiz, *Biochim. Biophys. Acta* **2003**, *1611*, 91; e) G. Francius, S. Dufour, M. Deleu, M. Paquot, M.-P. Mingeot-Leclercq, Y. F. Dufrêne, *Biochim. Biophys. Acta* **2008**, *1778*, 2058; f) C. Déjugnat, O. Diat, T. Zemb, *Chem. Phys. Chem.* **2011**, *12*, 2138; g) S. Buchoux, J. Lai-Kee-Him, M. Garnier, P. Tsan, F. Besson, A. Brisson, E. J. Dufourc, *Biophys. J.* **2008**, *95*, 3840.
[20] S. J. Rehm, A. Tice, *Clin. Infect. Dis.* **2010**, *51*, S176.
[21] D. G. Duff, A. Baiker, P. P. Edwards, *Langmuir* **1993**, *9*, 2301.
[22] a) A. Das, T. Li, G. Li, K. Nobusada, C. Zeng, N. L. Rosi, R. Jin, *Nanoscale* **2014**, *6*, 6458; b) C. Zeng, C. Liu, Y. Chen, N. L. Rosi, R. Jin, *J. Am. Chem. Soc.* **2014**, *136*, 11922; c) Q. Tang, D. Jiang, *J. Phys. Chem. C* **2015**, *119*, 2904; d) S. Chen, S. Wang, J. Zhong, Y. Song, J. Zhang, H. Sheng, Y. Pei, M. Zhu, *Angew. Chem., Int. Ed.* **2015**, *54*, 3145; e) C. Zeng, H. Qian, T. Li, G. Li, N. L. Rosi, B. Yoon, R. N. Barnett, R. L. Whetten, U. Landman, R. Jin, *Angew. Chem. Int. Ed.* **2012**, *51*, 13114.
[23] a) H.-Ch. Weissker, H. B. Escobar, V. D. Thanthirige, K. Kwak, D. Lee, G. Ramakrishna, R. L. Whetten, X. López-Lozano, *Nat. Commun.* **2014**, *5*, 3785; b) G. Li, Z. Lei, Q.-M. Wang, *J. Am. Chem. Soc.* **2010**, *132*, 17678; c) M. S. Devadas, V. D. Thanthirige, S. Bairu, E. Sinn, G. Ramakrishna, *J. Phys. Chem. C* **2013**, *117*, 23155.
[24] a) Z. Luo, X. Yuan, Y. Yu, Q. Zhang, D. T. Leong, J. Y. Lee, J. Xie, *J. Am. Chem. Soc.* **2012**, *134*, 16662; b) X. Le Guevel, O. Tagit, C. E. Rodríguez, V. Trouillet, M. Pernia Leal, N. Hildebrandt, *Nanoscale* **2014**, *6*, 8091; c) T. D. Green, C. Yi, C. Zeng, R. Jin, S. McGill, K. L. Knappenberger Jr., *J. Phys. Chem. A* **2014**, *118*, 10611; d) K. Pyo, V. D. Thanthirige, K. Kwak, P. Pandurangan, G. Ramakrishna, D. Lee, *J. Am. Chem. Soc.* **2015**, *137*, 8244.
[25] J. Zheng, C. Zhou, M. Yu, J. Liu, *Nanoscale* **2012**, *4*, 4073.
[26] a) W.-Y. Chen, C.-C. Huang, L.-Y. Chen, H.-T. Chang, *Nanoscale* **2014**, *6*, 11078; b) X. Wen, P. Yu, Y.-R. Toh, J. Tang, *J. Phys. Chem. C* **2012**, *116*, 11830.
[27] a) K. G. Stamplecoskie, Y.-S. Chen, P. V. Kamat, *J. Phys. Chem. C* **2014**, *118*, 1370; b) Z. Wu, R. Jin, *Nano Lett.* **2010**, *10*, 2568; c) Y. Chen, T. Yang, H. Pan, Y. Yuan, L. Chen, M. Liu, K. Zhang, S. Zhang, P. Wu, J. Xu, *J. Am. Chem. Soc.* **2014**, *136*, 1686.
[28] O. S. Wolfbeis, *Chem. Soc. Rev.* **2015**, *44*, 4743.
[29] L. M. Fan, J.-M. Li, *J. Pharmacol. Toxicol. Methods* **2014**, *70*, 40.
[30] a) I. W. Hamley, *Chem. Commun.* **2015**, *51*, 8574; b) L. Liu, K. Xu, H. Wang, J. P. K. Tan, W. Fan, S. S. Venkatraman, L. Li, Y.-Y. Yang, *Nat. Nanotechnol.* **2009**, *4*, 457.
[31] T. Schneider, A. Müller, H. Miess, H. Gross, *Int. J. Med. Microbiol.* **2014**, *304*, 37.
[32] B. C. Hoefler, K. V. Gorzelnik, J. Y. Yang, N. Hendricks, P. C. Dorrestein, P. D. Straight, *Proc. Natl. Acad. Sci. USA* **2012**, *109*, 13082.
[33] P. A. V. Fernandes, I. R. de Arruda, A. F. A. B. dos Santos, A. A. de Araújo, A. M. S. Maior, E. A. Ximenes, *Braz. J. Microbiol.* **2007**, *38*, 704.
[34] Z. Nozhat, A. Asadi, S. Zahri, *J. Nanomater.* **2012**, *2012*, 526580.
[35] a) K. H. L. Kwan, X. Liu, M. K. T. To, K. W. K. Yeung, C.-M. Ho, K. K. Y. Wong, *Nanomed.: Nanotechnol. Biol. Med.* **2011**, *7*, 497; b) N. Duraipandy, R. Lakra, K. V. Srivatsan, U. Ramamurhy, P. S. Korrapati, M. S. Kiran, *J. Mater. Chem. B* **2015**, *3*, 1415.
[36] a) X. Yuan, M. I. Setyawati, D. T. Leong, J. Xie, *Nano Res.* **2014**, *7*, 301; b) X. Yuan, M. I. Setyawati, A. S. Tan, C. N. Ong, D. T. Leong, J. Xie, *NPG Asia Mater.* **2013**, *5*, e39; c) Y. Liu, L. Wang, C. Bu, G. Wang, Y. Zhang, S. Fang, W. Shi, *J. Nanomater.* **2015**, *2015*, 792095; d) X. Wang, W. Gao, W. Xu, S. Xu, *Mater. Sci. Eng., C* **2013**, *33*, 656.
[37] C. T. N. Pham, D. G. Thomas, J. Beiser, L. M. Mitchell, J. L. Huang, A. Senpan, G. Hu, M. Gordon, N. A. Baker, D. Pan, G. M. Lanza, D. E. Hourcade, *Nanomed.: Nanotechnol. Biol. Med.* **2014**, *10*, 651.
[38] A. E. Krausz, B. L. Adler, V. Cabral, M. Navati, J. Doerner, R. A. Charafeddine, D. Chandra, H. Liang, L. Gunther, A. Clendaniel, S. Harper, J. M. Friedman, J. D. Nosanchuk, A. J. Friedman, *Nanomed.: Nanotechnol. Biol. Med.* **2015**, *11*, 195.